Tm^{3+} Tellurite-Modified-Silica Glass Thin Films Fabricated Using Ultrafast Laser Plasma Doping

Billy D. O. Richards , Artitsupa Boontan , Thomas Mann, Eric Kumi Barimah, Christopher Russell ,
David P. Steenson , *Senior Member, IEEE*, and Gin Jose

Abstract—**Thin glass films have been produced by implanting Tm^{3+} doped and Tm^{3+}/Er^{3+} codoped tellurite glasses into silica substrates using ultrafast laser plasma doping for the first time. The resulting glass films had thicknesses of up to 2 μm, refractive indices of 1.5–1.65 and exhibited photoluminescence in the 1.5–2.1 μm wavelength region when excited with 808 nm and 976 nm laser diodes. The OH^- content of the silica glass substrate was also found to have an effect on the $Tm^{3+}: {}^3F_4$ photoluminescence lifetime in the modified thin glass film layer, with the high OH^- containing substrate exhibiting a shorter lifetime. Through optimization of the femtosecond laser ablation parameters, we have produced crack-free thin films of Tm^{3+} doped tellurite-modified silica glass layers with good thickness uniformities of ± 10 nm, and the refractive index of the modified layer is up to 13% higher than the bare substrate material.**

Index Terms—**Erbium, optical films, thulium, ultrafast optics.**

I. INTRODUCTION

ULTRAFAST laser plasma doping (ULPD) has recently been shown to be a viable method for the production of thin glass films with interesting properties. Notable features of the thin films fabricated using this method include the ability to produce a SiO_2 glass network which is modified with TeO_2 based glass without phase separation or crystallization [1], which is not normally possible through traditional glass fabrication techniques; and importantly doping of the tellurite-modified-silica glass layer with larger concentrations of Er^{3+} than is possible in pure silica without crystallization, clustering and the associated detrimental effects on Er^{3+} spectroscopy, resulting in a record high lifetime-density product of Er^{3+} ions in silica [1], [2]. The same benefits were found when applying the technique using a substrate of silica-on-silicon which is an important material for a range of photonic devices [3], and the tellurite-modified-silica material is compatible with CMOS manufacturing processes thanks to its stability up to temperatures of around 600 °C [4]. RBS, TEM and EDX analysis of thin films fabricated using ULPD revealed that the doped layer is amorphous, homogeneous and that a very well-defined boundary exists between the modified layer and the pristine silica substrate which is necessary for the production of step-index waveguides [1], [2]. Codoping of the modified layers can be achieved either by codoping the target glass, or by sequential ablation of separate singly-doped target glasses, providing additional flexibility of fabrication and the ability to produce bespoke doping profiles within the modified layers [2]. The benefits of using tellurite glass as a target material include its ability to dissolve higher concentrations of rare-earth ions than silica glass, resulting in potentially higher optical gains [1] and more compact devices due to the larger absorption and emission cross-sections of rare earth ions in tellurite compared to silicate, fluoride and germanate glasses [5]. The different Te-O structural units which make up tellurite glass also result in inhomogeneous broadening of rare earth ion photoluminescence bands and the possibility of yielding broadband gain devices [1], [5]. Rare earth doped tellurite glass in various forms has also been demonstrated to yield efficient and compact laser sources [6]. By using ULPD to create hybrid tellurite-silica glass material, it is possible to overcome some of tellurite glass' drawbacks, such as its physical and thermal fragility whilst retaining its ability to dissolve large rare earth ion concentrations without clustering [1]. In this work we employ the ULPD technique to produce thin films of tellurite-modified-silica glass containing Tm^{3+} with and without Er^{3+} codopant ions and assess their material and spectroscopic properties with a focus on the 1.8 μm photoluminescence from the $Tm^{3+}: {}^3F_4 \rightarrow {}^3H_6$ transition. Tm^{3+} and Tm^{3+}/Er^{3+} doped thin films are of interest for a range of applications such as miniature sensors [7]–[9] and broadband planar amplification and light generation devices [10]–[12].

II. EXPERIMENTAL

A. Target Glass Preparation

Two target glasses with the composition $(79-x)TeO_2 - 10ZnO - 10Na_2O - 1Tm_2O_3 - xEr_2O_3$ (x = 0, 0.5) mol. % were fabricated for use in the ULPD process, and are subsequently denoted TmTZN and TmErTZN. The samples were prepared using analytical grade precursor chemicals (TeO_2, ZnO, Na_2CO_3, Tm_2O_3, Er_2O_3) which were weighed and mixed before being melted in a gold crucible at 850 °C in an electric furnace for

B. D. O. Richards, A. Boontan, T. Mann, E. Kumi Barimah, and G. Jose are with the Applied Photon Science Group, School of Chemical and Process Engineering, University of Leeds, Leeds LS2 9JT, U.K. (e-mail: b.d.o.richards@leeds.ac.uk; pm17a4b@leeds.ac.uk; mn14tm@leeds.ac.uk; e.kumi-barimah@leeds.ac.uk; g.jose@leeds.ac.uk).

C. Russell and D. P. Steenson are with the School of Electronic and Electrical Engineering, University of Leeds, Leeds LS2 9JT, U.K. (e-mail: c.russell@leeds.ac.uk; d.p.steenson@leeds.ac.uk).

Color versions of one or more of the figures in this paper are available online at http://ieeexplore.ieee.org.

TABLE I
SAMPLE FABRICATION DETAILS

Sample ID	Target Glass	Substrate	Average laser energy at the target (μJ)	Average laser fluence at the target (J/cm²)	Deposition duration (hrs)
TmSp1	TmTZN	Spectrosil 2000	210	3.0	1.5
TmSp2	TmTZN	Spectrosil 2000	235	3.4	5
TmIn3	TmTZN	Infrasil 301	215	3.1	6
TmIn4	TmTZN	Infrasil 301	150	2.1	5
TmErIn5	TmErTZN	Infrasil 301	240	3.4	6

3 hours under an atmosphere of flowing (1 l/min) oxygen gas. The melts were cast into preheated brass moulds and annealed at 295 °C for 3 hours before being cooled to room temperature at 0.5 °C/min. The resulting glass samples with dimensions of $30 \times 30 \times 5$ mm were then polished prior to characterization and ULPD processing.

B. Thin Film Preparation

Thin glass films were fabricated by focusing an ultrafast laser, (Wyvern, KM Labs) with a pulse duration of 45 fs, repetition rate of 1 kHz and peak wavelength of 800 nm onto a target tellurite glass which was placed in a custom pulsed laser deposition chamber (PVD Products), in which a 70–80 mTorr O_2 atmosphere was maintained. The focused laser beam had an elliptical spot with an area of approximately 7×10^{-5} cm² at the target surface. The material which was ablated from the target glass then deposited onto the surface of a $20 \times 30 \times 1.1$ mm Spectrosil 2000 or Infrasil 301 (Heraeus) silica glass substrate which was placed 70 mm above the target glass and was heated to 750 °C. The laser beam was rastered across the surface of the target glass at a rate of 5 mm/s and the substrate was rotated at 5 rpm. Table I details the specific fabrication properties for the tellurite-modified-silica thin films prepared for this work. The threshold fluence for laser ablation of TZN glass using a 100 fs, 800 nm laser has recently been found to depend on the laser spot size as well as the number of pulses which are incident on a given area of the target, with a larger spot size and greater number of pulses resulting in a lower ablation threshold fluence of around 0.14 J/cm², compared to 0.51 J/cm² for a single pulse with a smaller spot size. The addition of up to 1.5 mol. % Er^{3+} ions however, did not affect the ablation threshold of the glass [13]. In this work, we used laser fluences which were significantly higher than the ablation threshold for TZN glass.

The motivation behind using both Spectrosil 2000 and Infrasil 301 silica glass substrates was to investigate how the different substrate OH^- concentrations would affect the photoluminescence spectra and lifetime of the rare earth dopants. According to the manufacturer's datasheet, Spectrosil 2000 and Infrasil 301 contain ≤1300 ppm and ≤8 ppm OH^- ion contamination, and consequently exhibit 0% and 76% transmission at 2.7 μm, respectively, for a 10 mm thick sample [14]. The bottom level transition photoluminescence bands of both Tm^{3+} and Er^{3+} ions at 1.8 μm and 1.5 μm, respectively, are suggestive of suffering from quenching from OH^- ion impurity absorption bands in tellurite [5], [15], [16] and silicate glasses [17], [18].
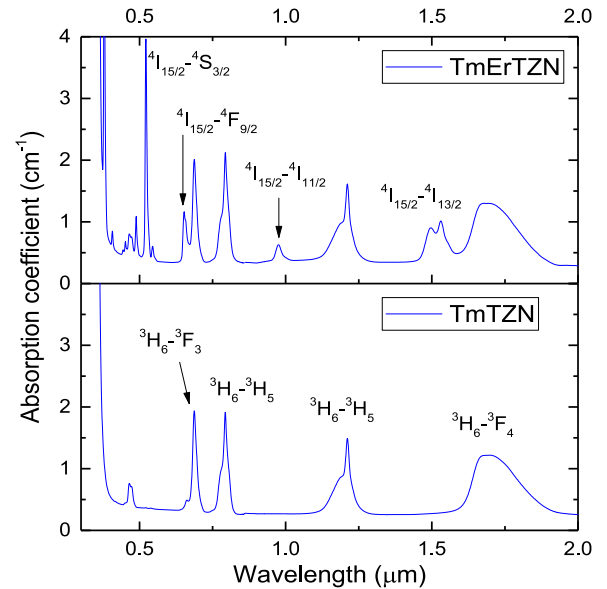

Fig. 1. Absorption spectra of the TmTZN and TmErTZN target glass samples doped with Tm^{3+} and Tm^{3+}/Er^{3+}, respectively. The bottom spectrum includes the designations of the main Tm^{3+} absorption transitions, while the top spectrum adds the transition designations for Er^{3+}.

C. Characterization

Absorption and transmission spectra were captured using UV-vis-NIR, (Lambda 950, Perkin Elmer) and FTIR (Vertex 90, Bruker) spectrophotometers. Photoluminescence spectra and lifetime measurements were made using a photoluminescence spectrometer (FLS920, Edinburgh Instruments) fitted with an InGaAs detector, and 808 nm and 976 nm laser diodes were used as excitation sources. Refractive index and thin film thickness measurements were made using a prism coupler (Model 2010, Metricon) fitted with a 633 nm HeNe laser. Surface analysis of thin films was performed using an atomic force microscope (AFM) operating in tapping mode (D3100, Veeco Digital Instruments, with a Nanoscope IVa controller and 14 nm nominal tip diameter). AFM data was analysed with the open source software Gwyddion [19].

III. RESULTS AND DISCUSSION

A. Absorption/Transmission Spectroscopy

The absorption spectra of the target glass samples used to fabricate the thin films are shown in Fig. 1, and the Tm^{3+} and Er^{3+} energy level transitions responsible for the main peaks
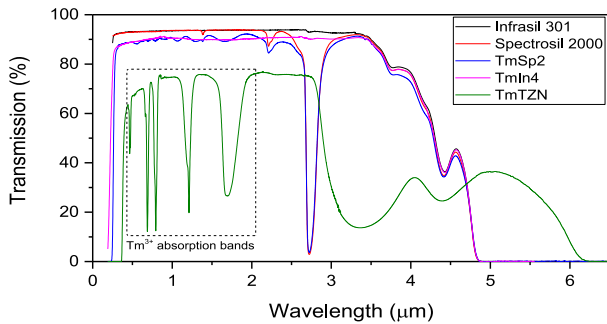
Fig. 2. Transmission spectra of the Tm^{3+} doped thin film samples TmSp2 and TmIn4, the target glass TmTZN and the blank Infrasil 301 and Spectrosil 2000 substrates. The spectra have not been corrected for reflection losses. (All samples are 1.1 mm thick except TmTZN which is 4.7 mm thick).

have been labeled. It should be noted that Er^{3+} also exhibits an absorption band at around 800 nm due to the $Er^{3+}: {}^4I_{15/2} \rightarrow {}^4I_{9/2}$ transition, however it is less intense than the Tm^{3+} absorption at the same wavelength [20], and is therefore obscured in the absorption spectrum. Example thin film transmission spectra of the Tm^{3+} doped samples TmSp2 and TmIn4 are shown in Fig. 2, comparing thin films deposited on Spectrosil 2000 and Infrasil 301 substrates where the former exhibits OH^- absorption bands at 2.2 μm and 2.7 μm. The rare earth ion absorption bands are not visible due to the thin nature of the doped layers. Interference fringes due to the doped layer are visible in the TmSp2 transmission spectrum, however, the transmission spectrum for sample TmIn4 does not show obvious interference fringes, and this is likely because the doped layer has a relatively low refractive index compared to TmSp2 (see section C). For comparison, the transmission spectrum of the TmTZN tellurite target glass shown in Fig. 2 exhibits a main OH^- absorption band which is significantly broader than in the silica glass and is shifted to a longer wavelength of 3.37 μm. The TmTZN target glass transmission spectrum also reveals the Tm^{3+} absorption bands described in Fig. 1. The sharp transmission cut-on edge of the thin film spectra at 270 nm provide evidence that the films are of good quality and free from crystallization or phase separation which would result in reduced transmission in the short wavelength visible region due to Rayleigh scattering. For further comparison, the transmission spectra of the bare Spectrosil 2000 and Infrasil 301 substrate materials are also shown in Fig. 2. The differences in the maximum transmission of the different samples are mainly due to the variations in sample refractive indices resulting in different values of Fresnel reflections from the surfaces which the transmission spectra in Fig. 2 have not been corrected for. The refractive indices (measured at a wavelength of 633 nm) of the bare substrates, TmSp2, TmIn4 and TmTZN are 1.457, 1.650, 1.533 and 2.037, resulting in Fresnel reflections of 3.5%, 6.0%, 4.4% and 11.7%, respectively, for a single face. (For the thin film samples, one face is unmodified substrate and will therefore have Fresnel reflections of 3.5%).

B. Microscopy

The surfaces of the thin glass films were inspected using optical microscopy, and the deposited layers appeared to be of good
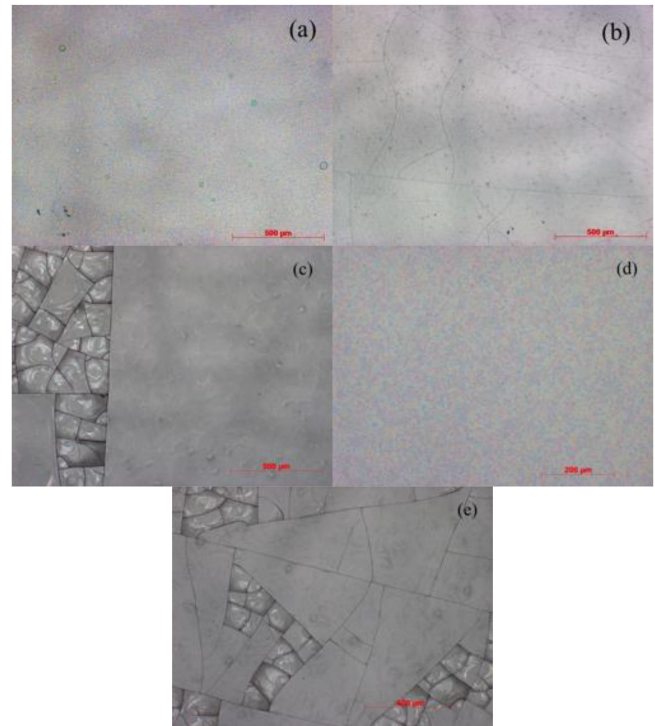

Fig. 3. Optical microscope images of the thin film sample surfaces: (a) TmSp1, (b) TmSp2, (c) TmIn3, (d) TmIn4 and (e) TmErIn5.

quality and homogeneous. However, the films produced with a high laser energy for 5 hours or longer show varying degrees of surface cracking, as can be seen in Fig. 3. The large amount of material deposition associated with long durations and high laser energies results in residual stress in the layer which subsequently causes cracking, whereas shorter depositions or lower laser energy results in high quality crack-free glass thin film layers. The susceptibility of thick layers to cracking is increased because of the coefficient of thermal expansion (CTE) mismatch between Spectrosil 2000 or Infrasil 301 (0.55×10^{-6} K^{-1} [14]) and TZN glass (19.8×10^{-6} K^{-1} [21]) and the elevated processing temperatures used in the ULPD technique. Residual stresses in the thin films may be alleviated to some extent by using thin films of silica-on-silicon as a substrate material, as silicon has an intermediate CTE value of around 4×10^{-6}–5×10^{-6} K^{-1} [22].

C. Refractive Index, Thickness and Surface Roughness Mapping

Fig. 4(a)–(c) shows contour plots of the refractive index (a, b) and thickness (c) of the TmSp2 thin film measured using prism coupling at a wavelength of 633 nm in TE (a) and TM (b) modes. Fig. 5 and Fig. 6 show the refractive index and thickness mapping of samples TmSp1 and TmIn4, respectively. Compared to TmSp2, TmSp1 was fabricated for a shorter duration, and TmIn4 was fabricated at a lower laser energy with all other parameters kept constant. As a result, both of the TmSp1 and TmIn4 layers are thinner than the TmSp2 layer and supported only a single mode during the prism coupling measurements, and individual TE and TM measurements of refractive index and thickness were therefore not possible. The black dots in the
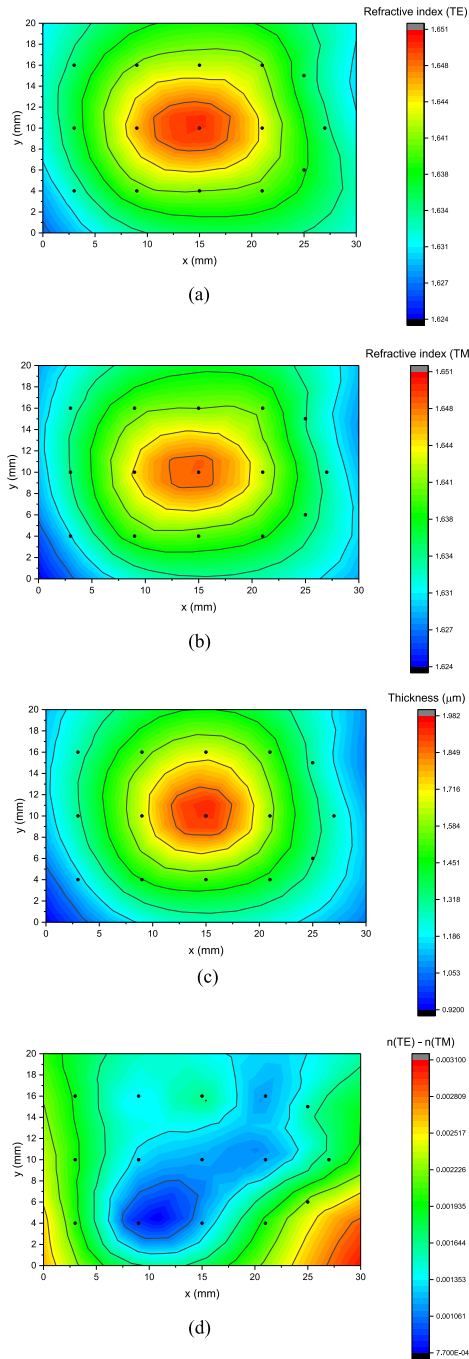
Fig. 4.   Refractive index (a, b) and thickness (c) mapping of sample TmSp2 measured in TE (a) and TM (b) modes using a 633 nm HeNe laser source. (d) Difference in refractive index measured in TE and TM modes (n(TE)–n(TM)).
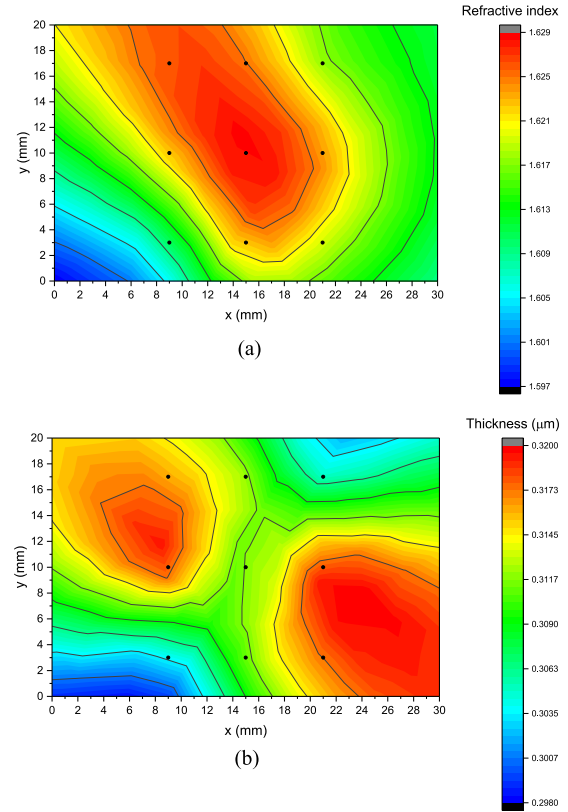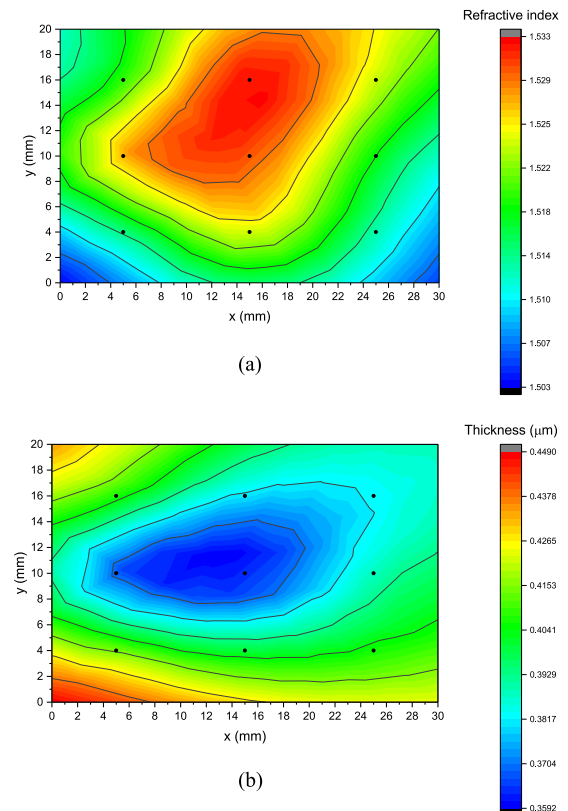

Fig. 5.   Refractive index (a) and thickness (b) mapping of sample TmSp1 using a 633 nm HeNe laser source.

Fig. 6.   Refractive index (a) and thickness (b) mapping of sample TmIn4 using a 633 nm HeNe laser source.

contour plots in Fig. 4–6 mark the positions of the measured data points, and the data has been extrapolated to the edges of the samples, represented by the boundary of the plots. Limitations of the equipment prevent the ability to take measurements very close to the edge of the sample. The measurements clearly show that TmSp2 was thicker and had a higher refractive index in the center of the sample, and this could also be seen by eye in the form of concentric interference fringes in the thin film surface. Fig. 4(d) shows the difference in refractive index

TABLE II
REFRACTIVE INDEX AND THICKNESS DETAILS

	TmSp1			TmSp2			TmIn4		
	n	Δn	t	n	Δn	t	n	Δn	t
Maximum value	1.630	11.8%	0.32 μm	1.650	13.2%	1.98 μm	1.533	5.2%	0.42 μm
Variation	0.020	-	0.02 μm	0.018	-	0.83 μm	0.020	-	0.06 μm
Variation (as % of max value)	1.2%	-	5.2%	1.1%	-	42.0%	1.3%	-	13.6%

Variation of the refractive index (n), refractive index increase compared to the substrate (Δn) and thickness (t) values measured across the surface of the samples TmSp1, TmSp2 and TmIn4.

measured in TE and TM modes (n(TE) – n(TM)), giving an indication of the sample birefringence, which appears to be larger towards the edges of the sample possibly due to residual stress in the material as a result of the thickness variation. Table II shows that the refractive index variation is similar for all three samples (1.1–1.3%), with TmIn4 having a lower refractive index value. This suggests that the lower material deposition rate associated with the lower laser energy results in the layer containing a smaller proportion of tellurite glass compared to silica glass within the modified layer, and that tuning of the layer refractive index should be possible by varying the material deposition rate. Good thickness uniformity, in the order of tens of nanometers, was also achieved in samples TmSp1 and TmIn4 when the deposition time was short or the laser energy was low, respectively. By comparison, TmSp2 exhibited large thickness variation of around 800 nm, which is suspected to be mainly due to the geometry of the rastering profile relative to the substrate concentrating the ablation plume towards the centre of the substrate. It is expected that thickness uniformity can be further improved for thicker samples by optimizing the rastering profile. Prism coupling of samples TmErIn5 and TmIn3 was not possible due to the surface cracking. Table II also compares the increase in the refractive index of the modified layer compared to the bare substrate material, with sample TmSp2 exhibiting a refractive index which is up to 13.2% higher than the substrate. In contrast, thin glass films fabricated via ion exchange exhibit refractive indices which are typically around 2% higher than the substrate [23].

The refractive index of the tellurite-modified-silica layer has previously been shown to increase with increasing rare earth ion concentration [1], and this was determined to be due to an increase in density of the modified layer due to the incorporation of heavy rare earth and tellurium ions in the silica glass network which is therefore more closely packed [2]. In tellurite glass however, increasing rare earth concentration (or decreasing TeO_2) concentration results in decreasing refractive index as can be seen in Fig. 7 where we have fabricated TZN glass samples in which TeO_2 was substituted with increasing concentrations of a mixture of Tm_2O_3, Er_2O_3 and Yb_2O_3, and also in TZN glass with varying Er_2O_3 concentration [24], despite the fact that the density of TZN glass increases with increasing rare earth ion concentration [1], [13]. However, due to its volatility, the concentration of tellurium found in the modified layer is lower than might be expected given its abundance in the target
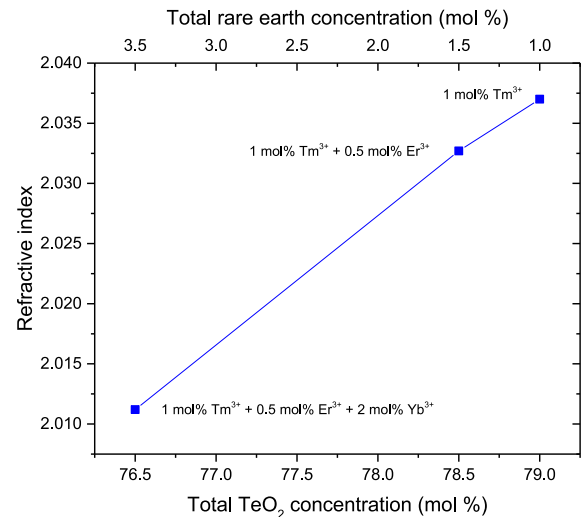

Fig. 7. Refractive index variation of TZN glass with varying total rare earth and TeO_2 concentrations.
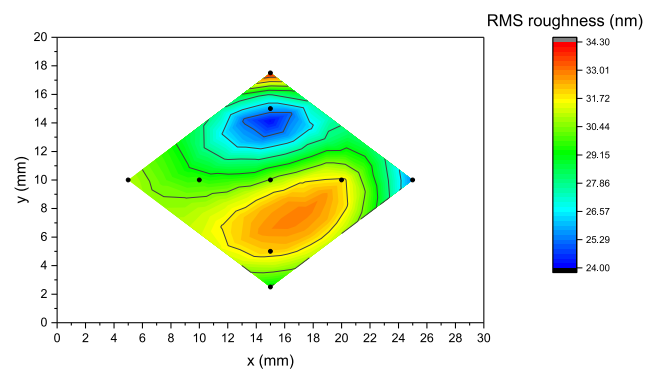

Fig. 8. Map of the RMS surface roughness of sample TmSp2.

glass [1], suggesting that the rare earth ions in the modified layers are predominantly in the silica glass network.

Fig. 8 shows a contour plot of the RMS surface roughness of sample TmSp2. Each data point, identified by a black dot in the contour plot, is the RMS surface roughness measured using AFM over a 100×100 μm section of the sample at that particular location. Over the region of the sample measured, the RMS surface roughness of the thin film layer varied in the range 24–34 nm, which is around 1.2% of the maximum film thickness.
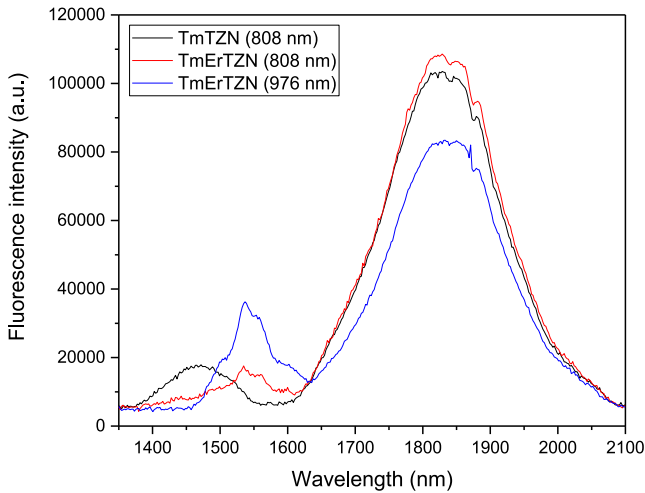
Fig. 9.   Photoluminescence spectra of the target glass samples used in this work when excited with 808 nm and 976 nm laser diodes.

D. Photoluminescence Spectroscopy

Fig. 9 shows the steady-state near-infrared photoluminescence spectra of the target glass samples when excited with either an 808 nm or 976 nm laser diode. As can be seen in the absorption spectra in Fig. 1, 808 nm light can be absorbed by the Tm^{3+}: $^3H_6 \rightarrow {}^3H_4$ and Er^{3+}: $^4I_{15/2} \rightarrow {}^4I_{9/2}$ transitions, while 976 nm light can be absorbed by the Er^{3+}: $^4I_{15/2} \rightarrow {}^4I_{11/2}$ transition. Near-infrared photoluminescence was observed in all cases except 976 nm excitation of the Tm^{3+} single doped sample, which is to be expected since Tm^{3+} does not have an absorption band at 976 nm. In all other cases, an intense photoluminescence peak centered at around 1820 nm from the Tm^{3+}: $^3F_4 \rightarrow {}^3H_6$ transition was observed. For the Tm^{3+} singly doped sample, when excited at 808 nm, there is an additional photoluminescence peak located at 1460 nm from the Tm^{3+}: $^3H_4 \rightarrow {}^3F_6$ transition, however, upon the addition of Er^{3+} ions, this peak reduces in intensity and a peak at 1535 nm from the Er^{3+}: $^4I_{13/2} \rightarrow {}^4I_{15/2}$ transition is observed. This implies that there is an efficient Tm^{3+}: $^3H_4$, Er^{3+}: $^4I_{15/2} \rightarrow Tm^{3+}$: $^3F_4$, Er^{3+}: $^4I_{13/2}$ energy transfer cross-relaxation process. The fact that intense 1820 nm photoluminescence is exhibited from the Tm^{3+}/Er^{3+} codoped sample under 976 nm excitation also confirms an energy transfer process from the Er: $^4I_{13/2}$ level to the Tm^{3+}: $^3F_4$ level. Under 976 nm excitation, the 1460 nm Tm^{3+}: $^3H_4 \rightarrow {}^3F_6$ transition is not visible, and the 1535 nm Er^{3+}: $^4I_{13/2} \rightarrow {}^4I_{15/2}$ transition is enhanced, suggesting that the Er^{3+}: $^4I_{13/2}$, Tm^{3+}: $^3F_4 \rightarrow Er^{3+}$: $^4I_{15/2}$, Tm^{3+}: $^3H_4$ energy transfer cross-relaxation process is less efficient than the reverse process (described above) under these conditions, and that ~800 nm excitation is preferable to ~980 nm excitation for broadband 1400–1600 nm amplifier applications. These excitation and energy transfer processes are summarized in the energy level diagram displayed in Fig. 10.

Fig. 11(a) compares the normalized near-infrared photoluminescence spectra and (b) lifetime of the 1.8 μm photoluminescence peak of the Tm^{3+} singly doped target glass and thin films fabricated using it on Spectrosil 2000 and Infrasil 301 substrate materials upon 808 nm excitation. The shape of the
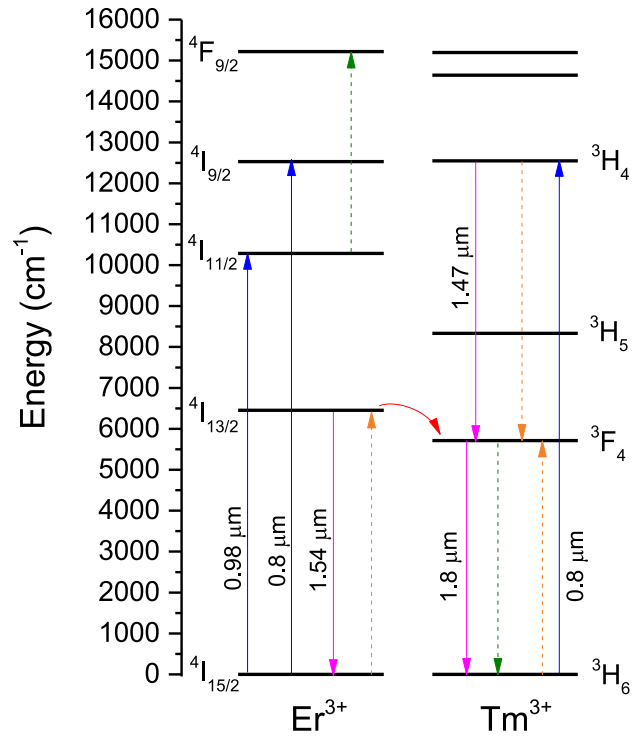

Fig. 10.   Energy level diagram for Tm^{3+} when codoped with Er^{3+}. Blue, pink and red arrows represent excitation, photoluminescence and energy transfer, respectively, while the dashed arrows represent energy transfer cross-relaxation processes.

Tm^{3+}: $^3F_4 \rightarrow {}^3H_6$ photoluminescence peak at 1.8 μm is largely unchanged between the target glass sample and the resulting thin films, with the thin films exhibiting slightly larger FWHM values (231 nm and 217 nm) than the target glass (201 nm). Measured photoluminescence of the Tm^{3+}: $^3F_4 \rightarrow {}^3H_6$ band in silica glass has previously been shown to have a FWHM of approximately 300 nm [25], [26]. Conversely, Er^{3+} doped tellurite glass has a broader ground-state photoluminescence band than Er^{3+} silica glass, and hence thin films fabricated using ULPD exhibit significantly narrower photoluminescence bands than the target glasses used to fabricate them [1]. The ULPD thin-film fabrication process has been shown to result in mixing of the target and substrate glass networks, resulting in rare-earth dopant ions exhibiting spectroscopic features associated with existing in both glass networks [1], [2]. The Tm^{3+}: $^3H_4 \rightarrow {}^3F_4$ photoluminescence band at 1.47 μm which is visible in the target glass spectrum is not visible in either of the Tm^{3+} doped thin film spectra, suggesting that the $^3F_4$, $^3H_6 \rightarrow {}^3H_4$, $^3H_4$ two-for-one energy transfer cross-relaxation process is enhanced in the thin films. Fig. 11(b) shows that the 1.8 μm photoluminescence lifetime of the Tm^{3+} doped thin film on Spectrosil 2000 substrate has a shorter lifetime (315 μs) than the parent target glass (447 μs), while the thin film on the Infrasil 301 substrate has a comparable lifetime of 476 μs. This indicates that the Tm^{3+} ions are mixing with the substrate silica glass network and being quenched by the large concentration of OH^- ions in Spectrosil 2000. The lack of OH^- ions in Infrasil 301 results in the Tm^{3+} lifetime being determined mainly by the OH^- content of the target glass rather than substrate. It has been shown previously that the Tm^{3+}: $^3F_4 \rightarrow {}^3H_6$ transition suffers from
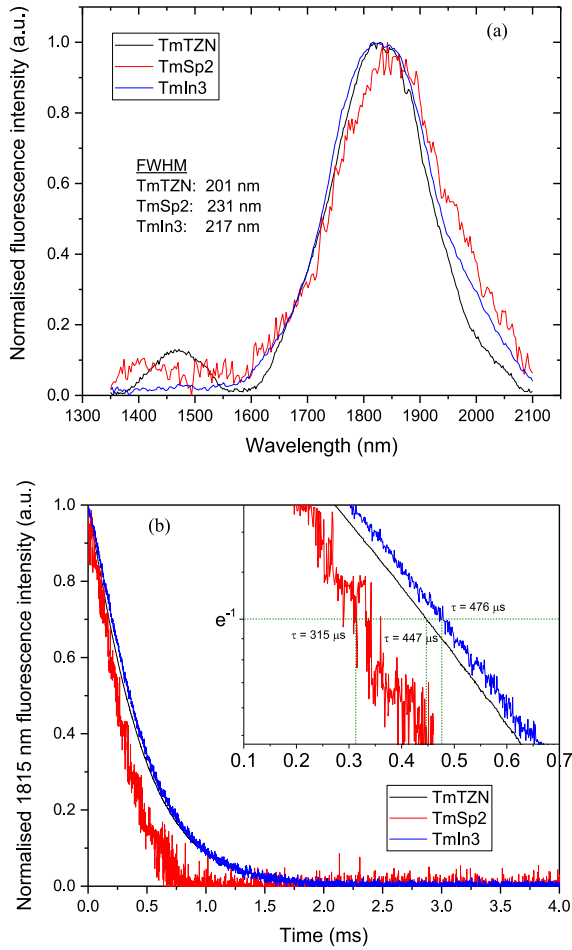
Fig. 11. (a) Normalized photoluminescence spectra and (b) 1.8 μm photoluminescence lifetime of the TmTZN target glass, TmSp2 and TmIn3 thin films when excited at 808 nm.

Fig. 12. Normalized photoluminescence spectra of Tm^{3+}/Er^{3+} codoped thin film sample TmErIn5 when excited with 808 nm and 976 nm laser diodes, and (inset) the normalized 1.8 μm photoluminescence decay curve when excited at 808 nm.

Er^{3+}: ^{4}I$_{11/2}$ $\rightarrow$ Tm^{3+}: ^{3}H$_6$, Er^{3+}: ^{4}F$_{9/2}$ energy transfer cross-relaxation process [10]–[12].

IV. CONCLUSION

In conclusion, we have prepared Tm^{3+} and Tm^{3+}/Er^{3+} doped thin films of tellurite-modified silica glass using ultrafast laser plasma doping for the first time, yielding layers up to 2 μm thick and with refractive indices of up to 1.65. By optimization of the laser parameters, crack-free films with good thickness uniformity were achieved, and further improvements are expected through optimization of the laser rastering scheme. The thin glass films exhibited strong photoluminescence from the Tm^{3+} ions at a wavelength of 1.8 μm which may be useful for sensing applications and miniature planar optical devices.

concentration quenching due to OH$^-$ ion impurities in tellurite glass, and that reducing the OH$^-$ ion concentration results in up to three times longer photoluminescent lifetime [5]. Clustering of Tm^{3+} ions in silica glass may also result in concentration quenching due to the enhancement of the ^{3}F$_4$, ^{3}F$_4$ $\rightarrow$ ^{3}H$_6$, ^{3}H$_4$ upconversion process [27], however, these results indicate that there is no evidence of clustering of Tm^{3+} ions in the tellurite-modified-silica glass thin film with up to 1 mol. % (2.7 wt. %) Tm^{3+} containing target glass, similar to Er^{3+} and Yb^{3+} doped thin films fabricated using the same method [1], [2].

Fig. 12 compares the normalized photoluminescence spectra of the Tm^{3+}/Er^{3+} codoped thin film sample (TmErIn5) when excited with 808 nm and 976 nm laser diodes. Under both excitation schemes, 1.8 μm photoluminescence is observed from the Tm^{3+}: ^{3}F$_4$ $\rightarrow$ ^{3}H$_6$ transition, however, the intensity is lower when using 976 nm excitation. Both excitation schemes also yield photoluminescence at 1.55 μm from the Er^{3+}: ^{4}I$_{13/2}$ $\rightarrow$ ^{4}I$_{15/2}$ transition but it is significantly weaker than is observed from the target bulk glass as shown in Fig. 9. The lifetime of the 1.8 μm photoluminescence from the Tm^{3+}/Er^{3+} doped TmErIn5 thin film sample under 808 nm excitation (Fig. 12 inset) is shorter than in the singly Tm^{3+} doped thin film samples which may be due to quenching from the Tm^{3+}: ^{3}F$_4$,
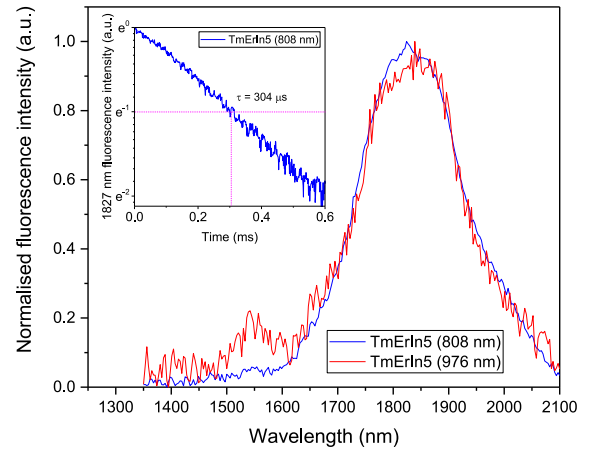
REFERENCES

[1] J. Chandrappan *et al.*, "Target dependent femtosecond laser plasma implantation dynamics in enabling silica for high density erbium doping," *Sci. Rep.*, vol. 5, 2015, Art. no. 14037.

[2] J. Chandrappan *et al.*, "Doping silica beyond limits with laser plasma for active photonic materials," *Opt. Mater. Exp.*, vol. 5, no. 12, pp. 2849–2861, 2015.

[3] S. A. Kamil *et al.*, "Ultrafast laser plasma doping of Er3+ ions in silica-on-silicon for optical waveguiding applications," *Opt. Lett.*, vol. 41, no. 20, pp. 4684–4687, 2016.

[4] J. Chandrappan *et al.*, "Devitrification of ultrafast laser plasma produced metastable glass layer," *Scripta Materialia*, vol. 131, pp. 37–41, 2017.

[5] B. Richards *et al.*, "Tellurite glass lasers operating close to 2 mm," *Laser Phys. Lett.*, vol. 7, no. 3, pp. 177–193, 2010.

[6] B. Richards and A. Jha, "Lasers utilising tellurite glass-based gain media," in *Technological Advances in Tellurite Glasses (Springer Series in Materials Science)*, V. Rivera and D. Manzani, Eds., 2017, pp. 101–130.

[7] Z. Y. Zhang *et al.*, "Thulium-doped intrinsic fiber optic sensor for high temperature measurements (>1100 degrees C)," *Rev. Sci. Instrum.*, vol. 69, no. 9, pp. 3210–3214, 1998.

[8] F. J. Mcaleavey and B. D. Maccraith, "Diode-pumped thulium-doped zirconium fluoride fiber as a fluorescent source for water sensing," *Electron. Lett.*, vol. 31, no. 16, pp. 1379–1380, 1995.

[9] A. Pal *et al.*, "A high-Q low threshold thulium-doped silica microsphere laser in the 2 mm wavelength region designed for gas sensing applications," *Laser Phys. Lett.*, vol. 10, no. 8, 2013, Art. no. 085101.

[10] R. Balda, J. Fernandez, and J. M. Fernandez-Navarro, Study of broadband near-infrared emission in Tm3+-Er3+ codoped TeO2-WO3-PbO glasses," *Opt. Exp.*, vol. 17, no. 11, pp. 8781–8788, 2009.

[11] L. H. Huang *et al.*, "Broadband emission in Er3+-Tm3+ codoped tellurite fibre," *Opt. Exp.*, vol. 12, no. 11, pp. 2429–2434, 2004.

[12] R. R. Xu *et al.*, "Investigation on broadband near-infrared emission and energy transfer in Er3+-Tm3+ codoped germanate glasses," *Opt. Mater.*, vol. 33, no. 3, pp. 299–302, 2011.

[13] T. Mann *et al.*, "Femtosecond laser ablation properties of Er3+ ion doped zinc-sodium tellurite glass," *J. Appl. Phys.*, vol. 124, no. 4, 2018, Art. no. 044903.

[14] Heraeus, "Quartz glass for optics - data and properties," Apr. 2018. HQS-MO_01.7/E/04.2018.

[15] S. X. Dai *et al.*, "Concentration quenching in erbium-doped tellurite glasses," *J. Lumin.*, vol. 117, no. 1, pp. 39–45, 2006.

[16] R. Balda *et al.*, "Spectroscopy and concentration quenching of the infrared emissions in Tm3+-doped TeO2-TiO2-Nb2O5 glass," *Opt. Exp.*, vol. 15, no. 11, pp. 6750–6761, 2007.

[17] E. Snoeks, P. G. Kik, and A. Polman, "Concentration quenching in erbium implanted alkali silicate glasses," *Opt. Mater.*, vol. 5, no. 3, pp. 159–167, 1996.

[18] M. Li *et al.*, "Investigation on Tm3+-doped silicate glass for 1.8 mm emission," *J. Lumin.*, vol. 132, no. 7, pp. 1830–1835, 2012.

[19] D. Necas and P. Klapetek, "Gwyddion: an open-source software for SPM data analysis," *Central Euro. J. Phys.*, vol. 10, no. 1, pp. 181–188, 2012.

[20] H. Yamauchi, G. S. Murugan, and Y. Ohishi, "Optical properties of Er3+ and Tm3+ ions in a tellurite glass," *J. Appl. Phys.*, vol. 97, no. 4, 2005, Art. no. 043505.

[21] S. Manning, H. Ebendorff-Heidepriem, and T. M. Monro, "Ternary tellurite glasses for the fabrication of nonlinear optical fibres," *Opt. Mater. Exp.*, vol. 2, no. 2, pp. 140–152, 2012.

[22] A. V. Mazur and M. M. Gasik, "Thermal expansion of silicon at temperatures up to 1100 degrees," *J. Mat. Process. Technol.*, vol. 209, no. 2, pp. 723–727, 2009.

[23] G. Jose *et al.*, "Ag+-Na+ ion exchange from dilute melt: guidelines for planar waveguide fabrication on a commercial phosphate glass," *Opt. Mater.*, vol. 23, no. 3–4, pp. 559–567, 2003.

[24] M. R. Oermann *et al.*, "Index matching between passive and active tellurite glasses for use in microstructured fiber lasers: Erbium doped lanthanum-tellurite glass," *Opt. Exp.*, vol. 17, no. 18, pp. 15578–15584, 2009.

[25] S. D. Jackson and T. A. King, "Theoretical modeling of Tm-doped silica fiber lasers," *J. Lightw. Technol.*, vol. 17, no. 5, pp. 948–956, 1999.

[26] S. D. Agger and J. H. Povlsen, "Emission and absorption cross section of thulium doped silica fibers," *Opt. Exp.*, vol. 14, no. 1, pp. 50–57, 2006.

[27] S. D. Jackson and S. Mossman, "Efficiency dependence on the Tm3+ and Al3+ concentrations for Tm3+-doped silica double-clad fiber lasers," *Appl. Opt.*, vol. 42, no. 15, pp. 2702–2707, 2003.

Billy D. O. Richards received the B.Sc. (Hons.) degree in engineering physics from Sheffield Hallam University, Sheffield, U.K., in 2002, and the Ph.D. degree in photonic materials from the University of Leeds, Leeds, U.K., in 2008. From 2008 to 2015 he was a Postdoctoral Research Fellow in the Institute for Materials Research, School of Process, Environmental and Materials Engineering, University of Leeds. In 2016, he joined a university spin-out company as a Senior Scientist, before joining the Applied Photon Science Group in the School of Chemical and Process Engineering, University of Leeds. His research interests include development and characterization of photonic materials such as glasses, fiber optics, thin films, waveguides, and laser gain media.

Artitsupa Boontan received the B.Eng. (Hons.) degree in nanomaterial engineering from King Mongkut's Institute of Technology Ladkrabang, Bangkok, Thailand, in 2015. She is currently working toward the M.Sc. degree in materials science and engineering at the School of Chemical and Process Engineering, University of Leeds, Leeds, U.K. From 2014 to 2015, she was a Research Assistant with the National Nanotechnology Centre, working on polymer light emitting diodes using ZnO nanowire arrays as electron transparent layers. In 2017, she received the Royal Thai Government Scholarship for study in the U.K.

Thomas Mann was born in London in 1992. He received the B.Sc. degree in physics from the University of Bristol, Bristol, U.K., in 2014. Since 2015, he has been working toward the Ph.D. degree in materials engineering at the Applied Photon Science Group, University of Leeds, Leeds, U.K.

His research interests include the development of an optical non-invasive glucose sensor, femtosecond laser-matter interactions and quantum optic dipole–dipole interactions.

Eric Kumi Barimah received the B.Sc. degree in physics from the Kwame Nkrumah University of Science and Technology, Kumasi, Ghana, in 2001, the M.S. degree in electrical engineering from Colorado Technical University, Colorado Springs, CO, USA, in 2007, and the Ph.D. degree from Hampton University, Hampton, VA, USA, in 2014. In 2015, he joined the School of Chemical and Process Engineering, University of Leeds, Leeds, U.K., as an Experimental Officer for the new Ultrafast Laser Plasma Implantation facility. His current research interests include using laser induced breakdown spectroscopy for optical sensing, and pulsed laser fabrication of glass/nanoparticles and polymer-based nanocomposite thin film for optical waveguide applications.

Christopher Russell received the B.Eng. degree in electronic and electrical engineering in 2009, and the Ph.D. degree in THz technologies in 2013 from the University of Leeds, Leeds, U.K.

Following a short continuation of the THz research in his first postdoctoral position, he realigned his microfabrication skills for neuroscience applications for defining electrical interfaces with the nerves for prosthetic limbs. He has since expanded his research in the area to include investigation of surface morphologies and novel applications of CMOS/MEMS technology in biological settings.

David P. Steenson (M'96–SM'08) received the B.Sc. (Hons.) degree in electronic and electrical engineering from the University of Manchester Institute of Science and Technology, Manchester, U.K., in 1984, and the Ph.D. degree from Nottingham University, Nottingham, U.K., in 1993.

From 1984 to 1988, he was a Microwave Development Engineer with Philips Microwave & Research Laboratories, and in 1993 he joined the University of Leeds, Leeds, U.K., where he is currently a Senior Lecturer. The main focus of his work is in the fabrication and applications of sub-millimeter wave electronic components, circuits and sub-systems, involving challenging device manufacture, nano-scale junctions and exacting embedding requirements both electrical and mechanical, i.e., ultra-low parasitics and three-dimensional micromachined circuit to device transitions via membrane in waveguide approaches. Other activities outside of this core high frequency interest include; co-integrated Er-ion doped thin-film glass on semiconductor approaches for all optical integrated subsystem development, fabrication of quantum cascade lasers, and the development of micro-machined vacuum tube components, and microfluidic and microelectrode arrays and manifolds for use in electro- and neuro-physiology research.

Gin Jose received the M.Sc. degree in physics from the University of Calicut, Calicut, India, in 1996, and the Ph.D. degree in physics from Mahatma Gandhi University, Kottayam, India, in 2003.

He was a Research Fellow with the Dipartimento di Fisica, Politecnico di Milano, Milan, Italy, from 2001 to 2002. He was a Senior Lecturer/Assistant Professor in physics with the Indian Institute of Technology, Guwahati, from 2003 to 2007. In 2007, he joined the School of Chemical and Process Engineering, University of Leeds, Leeds, U.K., where he is the Professor and Chair in functional materials since March 2013. He is currently leading the Applied Photon Science research group. He has research experience in the areas of novel laser glasses, photonic integration with dissimilar materials, glass thin films, pulsed laser processing of materials, sol–gel processing, laser spectroscopy, and ion-exchange with emphasis on applications in bio-chemical sensors/imaging, photonic components engineering, and energy applications.